Available online at www.sciencedirect.com
SCIENCE DIRECT®
ELSEVIER
Nuclear Instruments and Methods in Physics Research A 519 (2004) 222–229
NUCLEAR INSTRUMENTS & METHODS IN PHYSICS RESEARCH Section A
www.elsevier.com/locate/nima

# Simulation of a mirror corrector for PEEM3

W. Wan*, J. Feng, H.A. Padmore, D.S. Robin

*Advanced Light Source, Lawrence Berkeley National Laboratory, Berkeley, CA 94720, USA*

**Abstract**

A third generation aberration-corrected Photoemission Electron Microscope is being designed at the Advanced Light Source. An electron mirror is used for the correction of the lowest order spherical and chromatic aberrations. Two very different methods, one using finite-element method and ray-tracing technique and the other using charge ring method and differential algebra technique, have been employed to simulate the electrostatic field and the behavior of the electron beam. Good agreement has been obtained between the two methods and a tetrode mirror has been found to effectively correct the spherical and chromatic aberrations. Operating at 20 kV, the point resolution for 100% transmission reaches 50 nm with the mirror corrector, a significant reduction from that of 440 nm without correction. The highest resolution achieved is 4 nm at 2% transmission, as opposed to 20 nm at 1% transmission without correction.
© 2003 Elsevier B.V. All rights reserved.

*PACS:* 42.15.F; 07.78; 41.85

*Keywords:* XPEEM; Aberration correction; Electron mirror; Differential algebra

## 1. Introduction

The success of the X-ray excited Photoemission Electron Microscope (XPEEM) in recent years both at the Advanced Light Source and around the world [1] has generated the demand for a new generation of Photoemission Electron Microscopes (PEEMs) with a higher spatial resolution and transmission. The current generation of PEEM consists of mainly an objective lens, which accelerates the secondary electrons from a few electronvolts to 10–20 keV forming an intermediate image, and a set of projector lenses, which magnifies the intermediate image and forms the final image on the detector. The performance of such a device can be represented by that of the PEEM2 currently in operation at the Advanced Light Source [1]. The best resolution it has reached is about 20 nm at 1% transmission and the resolution that can be routinely achieved is roughly 50 nm at a few percent transmission [2]. The desire of the user community is that the new generation of PEEMs should be able to reach 3–5 nm at 1–2% transmission and 20–50 nm at 10–20% transmission.

The resolution of the current generation of PEEMs is limited fundamentally by aberrations of the microscope. Specifically, the aberrations are mainly generated in the gap between the sample and the objective lenses where the angle and energy spread are large. Due to rotational

*Corresponding author.
*E-mail address:* wwan@lbl.gov (W. Wan).

0168-9002/$ - see front matter © 2003 Elsevier B.V. All rights reserved.
doi:10.1016/j.nima.2003.11.159

symmetry, the lowest order spherical and chromatic aberrations are third- and first-order aberrations, respectively. They are the main limiting aberrations. In addition, the so-called Scherzer's theorem [3] states that neither the first-order chromatic nor the third-order spherical aberration changes sign in an optical device that preserves the rotational symmetry, maintains the direction of the beam and is free of space charges. As a result, the only way to reduce those two terms is to minimize them in each lens by adjusting the geometry of the electrodes.

To satisfy the demand of the users in improving the resolution or transmission by an order of magnitude, the first-order chromatic and third-order spherical aberrations have to be corrected. Since introducing the space charges is not an option in electron microscopes, the two remaining techniques are the use of multipoles, which breaks the rotational symmetry, and of electron mirrors, which changes the direction of the electron beam. Aberration correction using multipole correctors has been demonstrated in a Scanning Electron Microscope (SEM) [4] and Transmission Electron Microscopes (TEM) [5,6] in recent years. Sub-Å resolution has been achieved in STEM [7]. Since the spherical and chromatic aberrations of a PEEM are much larger than that of either SEM or TEM, it seems that multipole correctors are not suited for the aberration correction in a PEEM. Up to now, an electron mirror is the only device known (through both simulation and experiment) to be able to correct chromatic and spherical aberrations of a PEEM [8–13]. Obviously, the use of electron mirrors implies that the rotational symmetry has to be broken, because bending devices (separator) have to be used to prevent the electron beam from traveling back to the sample.

Currently, there are two third-generation aberration-corrected PEEMs under construction in the world, namely the "Spectromicroscope for all Relevant Techniques" (SMART) at BESSY II [14] and PEEM3 at the Advanced Light Source (see Fig. 1). The two microscopes are similar in many ways, such as the overall layout and the geometry of the magnetic separator and the electron mirror. On the other hand, they are different in various aspects. The main differences lie in the objective lens and the inclusion of an energy filter. While the SMART has an Ω-type energy filter in the layout, the PEEM3 does not have an energy filter in the design, as spectroscopy will be performed by changing the photon energy, not by analyzing the electron kinetic energy; this greatly simplifies the design. Regarding the objective lens, the SMART one is a combination of magnetic and electrostatic lenses, whereas the one in PEEM3 is a pure electrostatic lens. From the optical point of view, a magnetic round lens helps to reduce the chromatic and spherical aberrations. From the scientific point of view, on the other hand, the presence of magnetic field on the sample precludes the possibility of studying magnetic materials. Since magnetism has been one of the

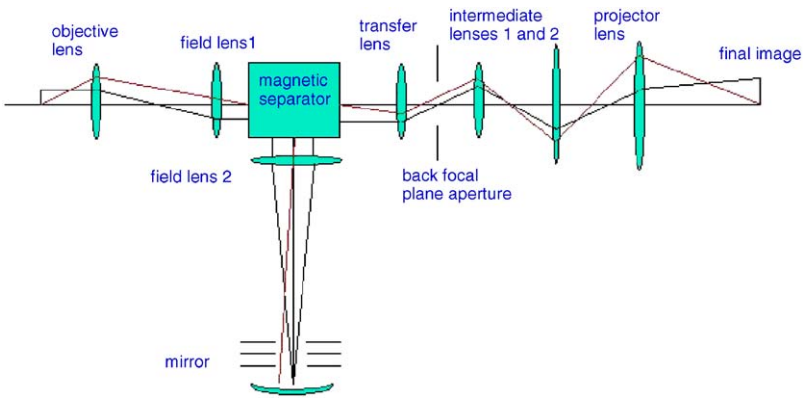


Fig. 1. The layout of PEEM3.

most exciting areas of research at PEEM2 and will remain so at PEEM3, a magnetic lens is not an option. The separator of PEEM3 is very similar to that of the SMART, with the same size and similar layout of coils [15]. The design of the mirror also follows closely that of the SMART [13], although the geometric dimensions are different. As shown schematically in Fig. 1, the mirror consists of four electrodes, which gives 3 free knobs to form an image and correct for the first-order chromatic aberration and the third-order spherical aberration simultaneously. An intermediate image is formed close to the bottom edge of the separator (Fig. 1) both before and after the mirror. Due to mirror symmetry, magnification between these two images (coinciding in space) can only be either $\pm 1$. In order to cancel coma generated by the mirror, the magnification is chosen to be $-1$ and a field lens is placed near the image to ensure that the linear optics is telescopic [16,17].

In this paper, the design of an electron mirror is presented. The numerical model of the mirror and the calibration of it are described in Section 2. The results of our simulation study and conclusions are presented in Section 3.

## 2. Numerical model

Over the past 60 years or so, numerous studies have been reported on the use of electron mirrors [18], which include both analytical and numerical works. Due to the great complexity of the field distribution inside a tetrode mirror, analytical expressions of aberration coefficients as integrals of derivatives of on-axis potential do not give enough information for finding the settings of the electrodes that give the desired focusing property and aberrations. More importantly, analytical theory lacks the power of predicting the range of the aberrations and the parameter dependence of the aberrations on the settings, the knowledge that is needed both at the design stage and during operation. Therefore, an accurate and efficient numerical model is needed to design such a mirror and to provide guidance for operation.

During the course of the design process, two different models were developed. The first one is based on a ray tracing code SIMION [19], which solves the electrostatic field using a finite element method and traces the motion of electrons using a Runge–Kutta integrator. It is very accurate, which was verified by benchmarking with known analytical solutions and other simulation codes and ultimately by comparing its result in the case of PEEM2 with the experimental data. The drawback is that, like all ray tracing codes, it is very slow. For example, it takes about 2 h to trace 12,800 electrons on a top of the line PC to the precision needed for accurate evaluation of low-order aberration coefficients. In spite of the apparent disadvantage, the first solution of a diode mirror that demonstrated the aberration correction in PEEM3 was found using this model.

In addition to the analytical theory and ray tracing, a third method, called the differential algebra (DA) has been developed. Instead of numerically solving the equations of motion for every particle, which is the case for ray tracing, it approximates the exact solution of the equations of motion with a set of Taylor series of arbitrary but finite order expanded around a certain reference trajectory. These Taylor series, which are final values of the phase space variables as functions of the initial values, are usually called Taylor maps. Unlike many other numerical models based on analytical perturbation theory which calculate the aberrations (coefficients in Taylor series) using analytical formulae, a DA model numerically solves the equations of motion once along the reference trajectory and obtains numerically ALL aberrations up to a given order. Tracking particles through these Taylor series takes little time compared to ray tracing. Using the same example above, it takes less than a minute to track the same 12,800 electrons. Furthermore, a DA model can examine dependence of aberrations on mirror parameters such as settings of the electrodes and geometrical dimensions of the mirror. Fast tracking and parameter dependence make feasible the statistical study of the effect of random errors of various sorts (for an example, see Ref. [15]). Parameter dependence of the aberrations on settings provides guidance for tuning an online model.

In order to develop a DA model of the mirror, an analytical model of the electrostatic field that is infinitely differentiable is needed. The constraint on differentiability ensures that a Taylor series of arbitrary oder can be obtained. Of the numerous ways of numerically solving rotationally symmetric electrostatic potential, charge ring method [20–23] satisfies the above requirement. The essence of this method is that the surface charge of the electrodes is represented by a set of discrete charge rings on or behind the surface. Following Ref. [24], charge rings in our model are placed behind the surface to avoid a singularity. Unlike finite element-type methods, the electrostatic potential of a charge ring can be expressed in an analytical form and the total potential is the sum over all charge rings. Assuming there are in total $n$ rings and the $i$th ring of charge $q_i$ and radius $r_i$ is located at $z_i$, the potential can be written as

$$u(r,z)=\frac{1}{2\pi^2\varepsilon_0}\sum_{i=1}^{N}\frac{q_iK(\tau_i)}{[(z-z_i)^2+(r+r_i)^2]^{1/2}} \tag{1}$$

where

$$K(\tau_i)=\int_0^{\pi/2}(1-\tau_i^2\sin^2\beta)^{-1/2}\,\mathrm{d}\beta \tag{2}$$

is the complete elliptic integral of the first kind, where $\beta$ is half the angle between the source and the point of interest in the cylindrical coordinates, and

$$\tau_i^2=\frac{4rr_i}{(z-z_i)^2+(r+r_i)^2}. \tag{3}$$

Since the potential on the surface of the electrodes is known, the charges of the rings can be obtained through solving a system of $n$ linear equations. Because $K(\tau_i)$ is divergent when $\tau_i$ approaches 1, i.e. $r$ and $z$ approaches $r_i$ and $z_i$, it is advantageous to place the charge rings behind the surface. To accommodate the potential need for parameter dependence on the geometry of the mirror, Taylor expansions of $K(\tau)$ are used for its evaluation [25], which are

$$K(\tau)=\frac{\pi}{2}\sum_{n=0}^{\infty}\left[\frac{(2n-1)!!}{2^n n!}\right]^2\tau^{2n} \tag{4}$$

$$K(\tau')=\ln\frac{4}{\tau'}+\sum_{n=1}^{\infty}\left[\frac{(2n-1)!!}{2^n n!}\right]^2\times\tau'^{2n}\left(\ln\frac{4}{\tau'}-\sum_{i=1}^{n}\frac{1}{i(2i-1)}\right). \tag{5}$$

Note that $\tau'=\sqrt{1-\tau^2}$.

The unique feature of an electron mirror is that the electrons are reflected in the mirror, which entails that, at the turning point, both the total momentum and the radius of curvature are small. Like most charged particle optics codes, the code on which our DA model of the mirror is based, COSY INFINITY [26], uses the arc length of the reference trajectory as the independent variable and slope type variable ($p_{x,y}/p_0$ in case of COSY) as transverse momentum. At the turning point, both local coordinates and transverse momentum become ill-defined. The problem can be circumvented by using time as the independent variable and $p_{x,y}/p_{0i}$ as transverse momentum, $p_{0i}$ is the total momentum of the reference particle before entering the mirror.

The model was tested extensively both before and during the design of the mirror. The charge ring model was first tested using a charged metal sphere and the relative uniformity of the potential on the surface is of the order $10^{-9}$. The equations of motion using time as the independent variable was initially benchmarked against the standard equations of motion in COSY using a $z$-dependent accelerating field and the agreement of aberrations up to the fifth-order is 7–8 digits. The first test of the full model of a mirror was done by comparing the results of a diode mirror [27] produced by COSY, SIMION and the SMART model. The relative uniformity of the potential on the surface is of the order $10^{-4}$ and the difference in potential between COSY and SIMION is below 3 V (out of 19.8 kV difference between the two electrodes) at 80% of the inner radius of the mirror. The difference in selected aberrations between the COSY and the SMART model is shown in Table 1. The agreement between SIMION and SMART model is even better. The 50% discrepancy in $c_{3c}$ was not pursued due to the lack of detailed information in Ref. [27] and the fact that it has little impact on the resolution of the microscope.

Table 1
The selected aberrations calculated by the SMART and COSY model

| | Defocus | $C_c$ | $C_s$ | $C_5$ | $C_{3c}$ | $C_{cc}$ |
|---|---|---|---|---|---|---|
| SMART (m) | 0 | 9.8256 | −539.71 | −904650 | 3272.6 | −5.4326 |
| COSY (m) | $-0.321 \times 10^{-4}$ | −9.9742 | 520.46 | 989923 | −4921.2 | 5.2229 |
| Difference (%) | −16(μm) | 1.51 | 3.57 | 9.43 | 50.38 | 3.86 |

Note that Defocus is the first-order term $(x|\alpha)$, $C_c$ is the first-order chromatic aberration $(x|\alpha\delta)$, $C_s$ is the third order spherical aberration $(x|\alpha^3)$, $C_5$ is the fifth-order spherical aberration $(x|\alpha^5)$, $C_{cc}$ is the second-order chromatic aberration $(x|\alpha\delta^2)$ and $C_{3c}$ is the fourth-order term $(x|\alpha^3\delta)$. $\delta$ is the relative energy deviation $\delta E_k/E_k$. Difference in Defocus is measured in terms of change in image position. The difference in the sign of all the coefficients is due to the opposite direction of $z$ axis. Note that the unit of the number in the first column and the last row is μm, not %.

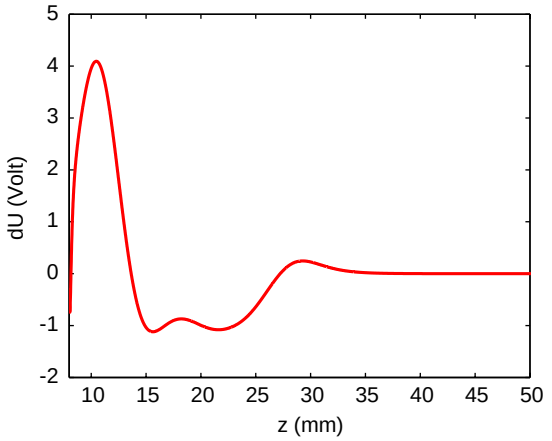


Fig. 2. Difference of the on-axis potential of the PEEM3 tetrode mirror between COSY and SIMION. The settings of the electrodes is a solution that minimizes $C_c$ and $C_s$ of the microscope. $V_1 = 20$ kV, $V_2 = 24.3355$ kV, $V_3 = 20$ kV and $V_4 = -4$ kV. All voltages are quoted relative to that of the sample, which is off ground. The subscripts of the voltages are defined in the caption of Fig. 3.

Finally, the COSY model of the tetrode mirror to be built in PEEM3 was benchmarked by the SIMION model. As shown in Fig. 2, the difference in the on-axis potential between the two models is below 4 V. The relative difference in the resolution after the mirror predicted by the two models is around 0.3% if the seventh-order map is used and around 0.6% if the third-order map is used.

## 3. Results and conclusion

The geometry of the tetrode mirror currently used for PEEM3 is shown in Fig. 3, along with the location of the charge rings (Table 2). Simulation study of the mirror and aberration correction done so far consists of mainly two parts. The first part is to determine the chromatic and spherical aberrations generated by the front end, which begins at

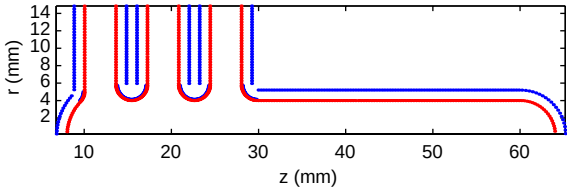


Fig. 3. Geometry of the tetrode mirror in PEEM3. The blue dots are the charge rings and the red dots are on the surface of the electrodes up to roughly $z = 40$ mm. From right to left, the electrodes are numbered 1, 2, 3 and 4, respectively. Actual dimensions are listed in Table 2. Note that the first (right most) electrode physically ends at roughly 33 mm. The extension shown here is a way to simplify the simulation. Otherwise the outer surface of the first electrode would have been included, which produces virtually the same field distribution but makes the geometry more complicated.

Table 2
Coordinates of all arcs in the tetrode mirror, which completely define the geometry of the mirror together with Fig. 3

| Electrode no. | Radius (mm) | $z_0$ (mm) | $r_0$ (mm) | $\phi_1$ (deg) | $\phi_2$ (deg) |
|---|---|---|---|---|---|
| 4 (arc 1) | 5.6 | 13.6 | 0 | 180 | |
| 136.7224 | | | | | |
| 4 (arc 2) | 1.8 | 8.2 | 5.0730 | −43.2776 | 0 |
| 3 | 1.8 | 15.4 | 5.8 | −180 | 0 |
| 2 | 1.8 | 22.6 | 5.8 | −180 | 0 |
| 1 | 1.8 | 29.8 | 5.8 | −180 | 90 |

Note that $z_0$ and $r_0$ are the longitudinal and radial coordinates of the center of an arc and $\phi_1$ and $\phi_2$ are the starting and ending angle of an arc.

the sample and ends at the entrance of the separator and is responsible for more than 95% of the total chromatic and spherical aberrations. Due to the tight schedule of the project, only the DA model of the mirror has been developed. The aberrations of the front end are determined experimentally. First, the distribution of electrons after the front end is obtained using the SIMION model, where the energy distribution of the secondary electrons $n_e$ is approximated by $n_e \sim E/(E + W_f)$ ($W_f$ is the work function of the sample) and the angle distribution is assumed to be uniform athmuzally and $\sim\cos\alpha$ radially [28]. Then, the electrons are tracked through a fake DA model of the mirror plus field lens which is simply a Taylor map that consists of a $-I$ linear matrix, together with the terms $C_c$ and $C_s$. The chromatic and spherical aberrations are varied until the minimum resolution is found. Resolution is defined as half the interval in $x$ (or $y$) that contains 68% of the total electrons. In order to determine the range of aberrations of PEEM3, a few extreme cases in terms of accelerating voltage and sample distance are identified and the aberrations are found (Table 3). In all calculations, the separator is assumed to be ideal, which is a unity matrix.

The second part is to find settings of the electrodes of the mirror that correct the aberrations and lead to a better resolution. Eventually the range of those aberrations that can be corrected by the mirror has to be obtained. Given the nonlinear nature of the mirror, weeks were devoted to the search. In the end a way of parameterization was developed which allows the mapping of the range of $C_c$ and $C_s$ to be done systematically. During the mapping process, the difference between $V_2$ and $V_3$ is fixed and $V_4$ is scanned and $V_3$ is varied accordingly to maintain the imaging condition. Thus a line in the $C_s$–$C_c$ plane is drawn. With different values of $V_2 - V_3$, different lines are drawn and the range of the mirror is mapped (see Fig. 4). What is not shown in Fig. 4 is that in part of the $C_s$–$C_c$ plane, there is another setting that gives the same $C_c$ and $C_s$. The problem of that branch of solutions is that it does not cover the range of $C_s$ and $C_c$ of the front end. The first setting of the mirror found to correct the aberrations effectively is part of that branch. It is inconceivable that the current settings with larger range in $C_s$ and $C_c$ can be found without the help of the DA model. With the settings that correct aberrations of each case (Table 4), resolution of these cases is obtained by tracking through the real mirror (see Table 3). The fact that the difference of resolution between the real and the fake mirror is small indicates that the other aberrations are small. Last but not the least, both $C_c$ and $C_s$ scale super linearly with image distance, providing a way of changing the range of the mirror without altering the geometry of the mirror. It is found numerically that, over the range of more than 15 cm, $C_c \sim d^{2.65}$, $C_s \sim d^{4.28}$, where $d$ is the distance between the flat surface of the mirror electrode to the image.

Using the DA model, a design of the electron mirror has been found for PEEM3. The mirror is able to correct aberrations of the microscope under all conditions of operation. With aberration correction, PEEM3 is likely to achieve the design goal of 5 nm at 1–2% transmission and 20 nm at 20–30% transmission. A detailed study of tolerances remains to be done. Yet the Taylor map of the mirror with parameter dependence in the setting of the electrodes already gives us a good indication of the stability requirement of the power supplies. First, according to the Taylor map, in the vicinity of the ideal setting, i.e. $\Delta V_i/V_i \sim 10^{-4} (i = 2, 3, 4)$, nonlinear dependence of $(x|\alpha)$, $C_c$ and $C_s$ on $\Delta V_i/V_i$ is negligible. Second, $\Delta(x|\alpha)$, $\Delta C_c/C_c$ and $\Delta C_s/C_s$ are all of the same

Table 3
Aberrations of the front end with various accelerating voltage and sample distance

| Cases | $C_c$ (m) | $C_s$ (km) | $R_o$ (nm) | $R_f$ (nm) | $R_r$ (nm) |
|---|---|---|---|---|---|
| 20 kV, 2 mm[a] | 41.1 | 14.0 | 423.9 | 48.7 | 49.9 |
| 20 kV, 2 mm | 41.0 | 14.0 | 421.7 | 48.7 | 50.1 |
| 20 kV, 5 mm | 51.3 | 9.35 | 1078.3 | 140.4 | 141.0 |
| 10 kV, 2 mm | 26.0 | 9.28 | 1111.5 | 162.5 | 168.7 |
| 10 kV, 5 mm | 28.3 | 9.35 | 2877.4 | 563.6 | 630.4 |

$R_o$, $R_f$ and $R_r$ are the resolution after the front end, after the fake mirror and after the real mirror, respectively. Tracking through the real mirror is done using a seventh-order map. All values of resolution are those with 100% transmission and axial rays only. The symbol 'a' marks the original solution.

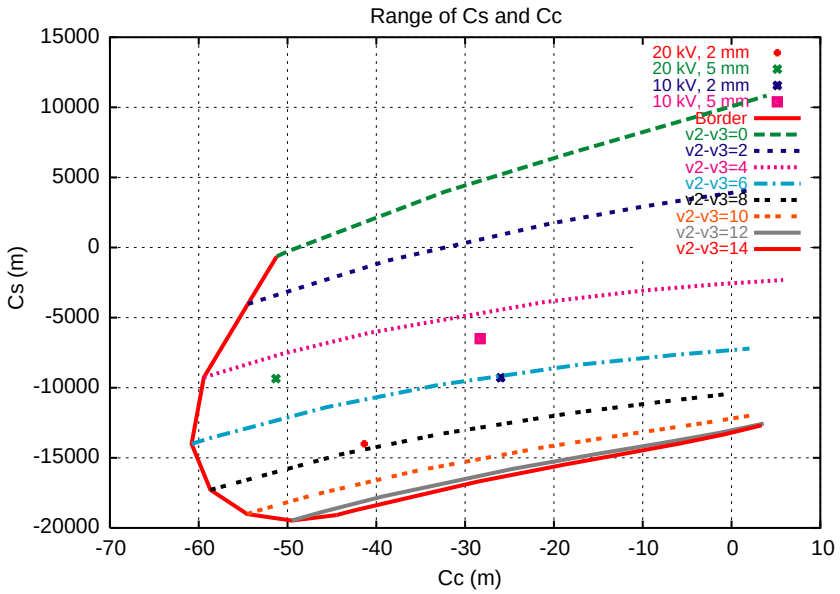


Fig. 4. The range in $C_c$ and $C_s$ of the front end and the mirror.

Table 4
Setting of the mirror that correct aberrations of the front end with various accelerating voltage and sample distance

| Cases | $C_c$ (m) | $C_s$ (km) | $V_1$ (kV) | $V_2$ (kV) | $V_3$ (kV) | $V_4$ (kV) |
|---|---|---|---|---|---|---|
| 20 kV, 2 mm* | 41.1 | 14.0 | 20.00000 | 24.33551 | 20.00000 | −4.00000 |
| 20 kV, 2 mm | 41.0 | 14.0 | 20.00000 | 10.72980 | 2.94704 | −1.89968 |
| 20 kV, 5 mm | 51.3 | 9.35 | 20.00000 | 7.78635 | 3.08963 | −1.58078 |
| 10 kV, 2 mm | 26.0 | 9.28 | 10.00000 | 4.19059 | 1.12565 | −0.94728 |
| 10 kV, 5 mm | 28.3 | 9.35 | 10.00000 | 3.52747 | 1.13595 | −0.87966 |

order of magnitude as $\Delta V_i/V_i$, which means that the tolerance on power supply ripple is limited by linear defocusing. Since $\alpha$ is of the order of 1 mrad, the change of 1 μm in $(x|\alpha)$ would result in the change of the resolution by 1 nm. Therefore, the power supplies of the mirror should be stable to the order of $10^{-6}$, which is consistent with the tolerance of the SMART mirror [14].

The work so far also indicates useful direction for further optimization of the mirror. In a 4 element mirror, $C_s$ and $C_c$ are intrinsically linked. $C_c$ is set by the penetration into the mirror field longitudinally, $C_s$ by the radial potential and both are changed by the $V_4$–$V_3$ potential. This suggests that a way to change the radial potential without significantly changing the axial potential near the mirror will separate $C_c$ and $C_s$. Such a system could be built by radially segmenting the mirror electrode or by using a mirror with a resistive coating with an applied potential between the central hole and the edge of the element.

## Acknowledgements

The authors would like to thank A. Doran, R. Duarte, N. Kelez, A. MacDowell, M. A. Marcus, D. Munson, H. Rose, R. Schlueter, A. Scholl and Y. Wu for numerous useful discussions.

## References


[1] S. Anders, H.A. Padmore, et al., Rev. Sci. Instr. 70 (1999) 3973 and references therein.
[2] A. Scholl, private communication.
[3] O. Scherzer, Z. Phys. 97 (1936) 593.
[4] J. Zach, M. Haider, Nucl. Instr. and Meth. A 363 (1995) 316.
[5] M. Haider, H. Rose, et al., Ultramicroscopy 75 (1998) 53.
[6] N. Dellby, O.L. Krivanek, P.D. Nellist, P.E. Batson, A.R. Lupini, J. Electron Microsc. 50 (2001) 177.
[7] P.D. Nellist, N. Dellby, O.L. Krivanek, M. Murfitt, Z. Szilagyi, Nucl. Instr. and Meth. A these Proceedings.
[8] G.F. Rempfer, J. Appl. Phys. 67 (1990) 6027.
[9] Z. Shao, X.D. Wu, Rev. Sci. Instr. 61 (1990) 1230.
[10] W.P. Skoczylas, G.F. Rempfer, O.H. Griffith, Ultramicroscopy 36 (1991) 252.
[11] G.F. Rempfer, M.S. Mauck, Optik 92 (1992) 3.
[12] G.F. Rempfer, D.M. Desloge, W.P. Skoczylas, O.H. Griffith, Microsc. Microanal. 3 (1997) 14.
[13] D. Preikszas, H. Rose, J. Electron Microsc. 46 (1997) 1.
[14] R. Fink, et al., J. Electron Spectrosc. Relat. Phenom. 84 (1997) 231.
[15] Y.K. Wu, et al., Nucl. Instr. and Meth. A, 2004, these Proceedings.
[16] H. Rose, D. Preikszas, Optik 92 (1992) 31.
[17] W. Wan, M. Berz, Phys. Rev. E 54 (1996) 2870.
[18] H. Rose, D. Preikszas, Nucl. Instr. and Meth. A 363 (1995) 301 and references therein.
[19] D.A. Dahl, J.E. Delmore, A.D. Appelhans, Rev. Sci. Instr. 61 (1990) 601.
[20] D.R. Cruise, J. Appl. Phys. 34 (1963) 3477.
[21] H.R. Lewis Jr., J. Appl. Phys. 37 (1966) 2541.
[22] H.A. Van Hoof, J. Phys. E: Sci. Instr. 13 (1980) 1081.
[23] A. Renau, F.H. Read, J.N.H. Brunt, J. Phys. E: Sci. Instr. 15 (1982) 347.
[24] G. Schönecker, R. Spehr, H. Rose, Nucl. Instr. and Meth. A 298 (1990) 360.
[25] I.S. Gradshtein, I.M. Ryzhik, A. Jeffrey, Table of Integrals, Series, and Products, Academic Press, Boston, 1994.
[26] M. Berz, COSY INFINITY Version 8.1 Users Guide and Reference Manual, MSUHEP-20704, Department of Physics and Astronomy, Michigan State University, 2002.
[27] D. Preikszas, P. Hartel, R. Spehr, H. Rose, Proceedings EUREM 12, Brno 2000, Brno, Czech Republic, Vol. III, p. I 81.
[28] B. Tonner, D. Dunham, Nucl. Instr. and Meth. A 347 (1994) 436.